電気学会論文誌●（●●●●●●●部門誌）
IEEJ Transactions on ●●●●●●●●●●●●●●●●
Vol.●● No.● pp.●-●● DOI: ●.●●/ieejeiss.●●.●

Paper

Stabilization Method for IPMSM with Long Electrical Time Constant Using Equivalent Resistance Gain Based on V/f Control

Jun-ichi Itoh*a), Senior member, Takato Toi*, Member, Koroku Nishizawa*, Student member

(Manuscript received Jan. 00, 20XX, revised May 00, 20XX)

This paper proposes a novel feedback control loop based on a damping control in a V/f control in order to stabilize interior permanent magnet synchronous motors (IPMSMs) with a long electrical time constant. A problem of the conventional damping control is that ignored roots move to the unstable region due to the conventional damping gain K_1. In addition, the ignored roots are apt to become unstable because of its long electrical time constant. Therefore, a novel method is proposed in order to solve this instability problem. In this paper, first, a boundary condition of stable region is derived based on state equation. Then, a novel current feedback loop of the current is added to an output voltage command. As experimental results, the motor becomes unstable with the conventional damping control under a rated speed of 0.9p.u. and a rated torque of 0.7p.u. Under the common operation condition, the motor is stabilized by employing the novel feedback control loop.

Keywords : Damping control, IPMSM, Root locus, V/f control

1. Introduction

Recently, interior permanent magnet synchronous motors (IPMSMs) are widely utilized due to their high efficiency and high power density(1)-(6). V/f control is generally employed for applications such as pumps and fans, where high dynamic performance is not demanded, because of its effectiveness and simplicity instead of a sensorless field-oriented-control(7)-(8).

In case that an open-loop V/f control without any feedback loop is applied for an IPMSM, persistent oscillation occurs in motor speed. Thus, the control system becomes unstable due to this oscillation. Therefore, the employment of the feedback loop of an active current is proposed as one of stabilizing methods(9). By suppressing the oscillation with this damping control, stable operation is achieved. In this method, the parameters of the damping control are decided by equations which are acquired from second-order state equation. In addition, the parameters of the damping control are calculated by an auto-tuning method. With this auto-tuning method, the motor parameters are not necessary in advance. However, due to the influence of ignored roots, this design method still cannot stabilize some IPMSMs because these roots move to the right in the s-plane in accordance with the increase of the conventional feedback loop gain K_1. In addition, the ignored roots are apt to become unstable in the long electrical time constant. In particular, the electrical time constant of a high-speed motor becomes long because of its small winding resistance. Therefore, a high-speed motor tends to become unstable based on V/f control with the conventional damping control using active current feedback.

In this paper, a novel feedback loop is proposed in order to solve the instability problem. The originality of this paper is an additional gain K_2 which is the gain in the proposed feedback loop in order to stabilize the high speed IPMSMs by increasing the winding resistance equivalently. The contribution of this paper is that the application of the V/f control is enlarged to the long electrical time constant IPMSM by adding a feedback loop.

This paper is organized as follows; first, the conventional damping control is introduced. Next, an auto-tuning method for the conventional damping control is explained. In addition, the stability of the V/f control is analyzed in order to clarify the boundary condition of the unstable region with the conventional damping control method. Next, the stability analysis is conducted with proposed feedback loop. From the experimental results, the equivalent resistance gain K_2 stabilizes the unstable V/f control system.

2. V/f Control for IPMSM

2.1 Damping Control Based on V/f Control Fig. 1 shows the relation between γδ-frame and dq-frame. The d-axis is defined as the direction of the flux vector of the permanent magnet. The q-axis is defined as the electro motive force vector. On the other hand, the V/f control is implemented on the γδ-frame. The δ-axis is aligned with the direction of the inverter output voltage, whereas

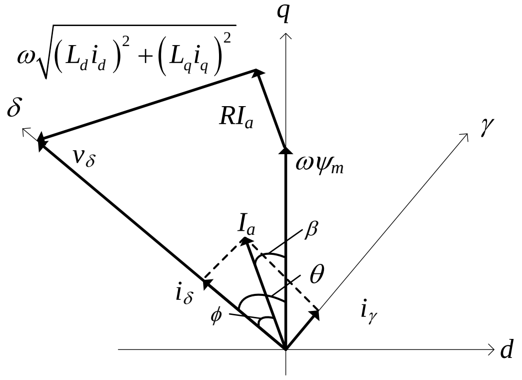

Fig. 1. Relation between γδ-frame and dq-frame.

a) Correspondence to: Jun-ichi Itoh. E-mail: itoh@vos.nagaokaut.ac.jp
* Nagaoka University of Technology.
1603-1, Kamitomioka-machi, Nagaoka, Niigata, Japan 940-2188

the γ-axis is defined as the δ-axis delayed by 90 degrees.

Fig. 2 shows the V/f control block diagram with the conventional damping control. The V/f control is based on the γδ-frame. The constant oscillation occurs in the high-speed region due to the resonance between the inertia of the motor and the inductance when the IPMSMs are driven by the open loop V/f control. Thus, the δ-axis current, which represents the active component, is utilized in order to stabilize the oscillation.

2.2 Conventional Design Method for Damping Control Based on V/f Control First, in order to analyze the stability of the V/f control, the IPMSM model at steady state is linearized. The linearized fifth-order state equation, which is expressed by (1) below, is derived from the following 4 equations: γδ-axis voltage equations (2), relational expression between torque and speed (3), relational expression between load angle and speed (4), and relational expression between input and output of HPF applied in damping control (5).

$$\begin{bmatrix} v_\gamma \\ v_\delta \end{bmatrix} = \begin{bmatrix} R + p\left(L_0 - L_1\cos 2\theta\right) - \omega_1 L_1 \sin 2\theta & pL_1 \sin 2\theta - \omega_1\left(L_0 + L_1 \cos 2\theta\right) \\ pL_1 \sin 2\theta + \omega_1\left(L_0 - L_1\cos 2\theta\right) & R + p\left(L_0 + L_1 \cos 2\theta\right) + \omega_1 L_1 \sin 2\theta \end{bmatrix} \begin{bmatrix} i_\gamma \\ i_\delta \end{bmatrix} + \omega\psi_m \begin{bmatrix} \sin\theta \\ \cos\theta \end{bmatrix} \quad \text{.......} \ (2)$$

$$p\omega = \frac{P_f^2}{J}\left\{\psi_m\left(i_\gamma \sin\theta + i_\delta \cos\theta\right) + \left(L_d - L_q\right)\left(i_\gamma \cos\theta - i_\delta \sin\theta\right)\left(i_\gamma \sin\theta + i_\delta \cos\theta\right)\right\} \quad \text{......} \ (3)$$

$$p\theta = \omega^* - K_1\left(i_\delta - x\right) - \omega \quad \text{..........} \ (4)$$

$$px = \left(i_\delta - x\right)\frac{1}{\tau} \quad \text{..........} \ (5)$$

where, i_γ is the γ-axis current, i_δ is the δ-axis current, ω is the motor speed, ω^* is the command value of motor speed, θ is the load angle, x is the output of integrator from high pass filter (HPF), p is the differential operator, R is the winding resistance, ψ_m is the field flux linkage, V_f is the f/v conversion ratio, K_1 is the damping gain, τ is the time constant of HPF, P_f is the number of pole pairs, and J is the inertia of the motor. Note that the definition of per unit value of K_1 is a product of rated speed and rated current (rad/sA). Furthermore, following approximations are used in the derivation for (1):

1) product of more than two perturbation (Δ) terms is 0, and
2) load angle perturbations are small; $\sin\Delta\theta = \Delta\theta$, $\cos\Delta\theta = 0$, when $\Delta\theta$ is small.

In addition, L_0 and L_1 are defined as

$$L_0 = \frac{L_d + L_q}{2}, \quad \text{..........} \ (6)$$

$$L_1 = \frac{L_q - L_d}{2}. \quad \text{..........} \ (7)$$

The state variables are i_γ, i_δ, ω, θ, and x. Root locus is obtained from fifth-order state equation. Note that the variables with subscription 0 mean the variables at the operating point.

Table 1 shows the motor parameters of two IPMSMs. In this paper, the stability of the two motors is analyzed. Note that the motor with a rated power of 3.7 kW is defined as Motor A, and the other is Motor B(10). In addition, electrical time constants $\%X_{Ld}/\%R$ and $\%X_{Lq}/\%R$ of Motor B are longer than that of Motor A by 7.6

$$p\begin{bmatrix} \Delta i_\gamma \\ \Delta i_\delta \\ \Delta\omega \\ \Delta\theta \\ \Delta x \end{bmatrix} = \begin{bmatrix}
\frac{-R\left(L_0 + L_1\cos 2\theta_0\right) + 2\omega_0 L_0 L_1 \sin 2\theta_0}{L_0^2 - L_1^2} & \frac{-K_1\left(L_0^2 - L_1^2\right)i_{\delta 0} + \omega_0\left(L_0^2 + 2L_0L_1\cos 2\theta_0 + L_1^2\right) + RL_1\sin 2\theta_0}{L_0^2 - L_1^2} & \frac{-\psi_m\left(L_0 - L_1\right)\sin\theta_0 + 2L_1^2 i_{\delta 0} + 2L_0L_1\left(i_{\gamma 0}\sin 2\theta_0 + i_{\delta 0}\cos 2\theta_0\right)}{L_0^2 - L_1^2} & \frac{-\omega_0\psi_m\left(L_0 + L_1\right)\cos\theta_0 + 2\omega_0 L_1^2 i_{\gamma 0} + 2\omega_0 L_0 L_1\left(i_{\gamma 0}\cos 2\theta_0 - i_{\delta 0}\sin 2\theta_0\right)}{L_0^2 - L_1^2} & K_1 i_{\delta 0} \\
\frac{-RL_1\sin 2\theta_0 + \omega_0\left(L_0^2 + L_1^2\right) - 2\omega_0 L_0 L_1 \cos 2\theta_0}{L_1^2 - L_0^2} & \frac{-K_1\left(L_0^2 - L_1^2\right)i_{\gamma 0} + 2L_0L_1\omega_0\sin 2\theta_0 + R\left(L_0 - L_1\cos 2\theta_0\right)}{L_1^2 - L_0^2} & \frac{\psi_m\left(L_0 - L_1\right)\cos\theta_0 + 2L_1^2 i_{\gamma 0} - 2L_0L_1\left(i_{\gamma 0}\cos 2\theta_0 - i_{\delta 0}\sin 2\theta_0\right)}{L_1^2 - L_0^2} & \frac{-\omega_0\psi_m\left(L_1 + L_0\right)\sin\theta_0 - 2\omega_0 L_1^2 i_{\delta 0} + 2\omega_0 L_0 L_1\left(i_{\gamma 0}\sin 2\theta_0 + i_{\delta 0}\cos 2\theta_0\right)}{L_1^2 - L_0^2} & -K_1 i_{\gamma 0} \\
\frac{P_f^2\psi_m}{J}\left\{\sin\theta_0 + \frac{1}{\psi_m}\left(L_d - L_q\right)\left(i_{\gamma 0}\sin 2\theta_0 + i_{\delta 0}\cos 2\theta_0\right)\right\} & \frac{P_f^2\psi_m}{J}\left\{\cos\delta_0 + \frac{1}{\psi_m}\left(L_d - L_q\right)\left(i_{\gamma 0}\cos 2\theta_0 - i_{\delta 0}\sin 2\theta_0\right)\right\} & 0 & \frac{P_f^2\psi_m}{J}\left\{i_{\gamma 0}\cos\theta_0 - i_{\delta 0}\sin\theta_0 - \frac{2\left(L_d - L_q\right)}{\psi_m} i_{\gamma 0} i_{\delta 0}\sin 2\theta_0 + \frac{L_d - L_q}{\psi_m}\left(i_{\gamma 0}^2\cos 2\theta_0 - i_{\delta 0}^2\cos 2\theta_0\right)\right\} & 0 \\
0 & -K_1 & -1 & 0 & K_1 \\
0 & \frac{1}{\tau} & 0 & 0 & -\frac{1}{\tau}
\end{bmatrix} \begin{bmatrix} \Delta i_\gamma \\ \Delta i_\delta \\ \Delta\omega \\ \Delta\theta \\ \Delta x \end{bmatrix} + \begin{bmatrix} i_{\delta 0} - \frac{L_1\sin 2\theta_0}{L_0^2 - L_1^2}V_f \\ -i_{\gamma 0} - \frac{L_0 - L_1\cos 2\theta_0}{L_1^2 - L_0^2}V_f \\ 0 \\ 1 \\ 0 \end{bmatrix}\Delta\omega^* \quad (1)$$

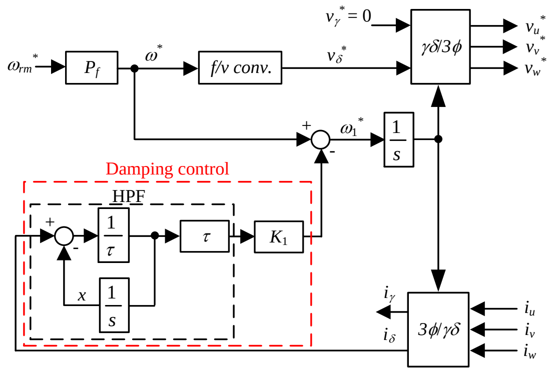

Fig. 2. Block diagram of V/f control based on γδ-frame with conventional damping control.

Table 1. Motor parameters of two IPMSMs.

	Motor A	Motor B
Rated mechanical power P_m	3.7 kW	3 kW
Rated speed ω_n	1800 r/min	12000 r/min
Rated current I_n	14 A	17.3 A
Number of pole pairs P_f	3	2
d-axis inductance L_d	6.2 mH	2.04 mH
q-axis inductance L_q	15.3mH	2.24 mH
Winding resistance R	0.69 Ω	0.133 Ω
Field flux linkage ψ_m	0.27 Vs/rad	0.107 Vs/rad
Inertia moment J	0.037 kgm^2	0.0013 kgm^2
Electrical time constant $\%X_{Ld}/\%R$	5.05	38.5
Electrical time constant $\%X_{Lq}/\%R$	12.5	42.3

times and 3.4 times.

Fig. 3 shows the eigenvalue plot of the Motor A when the damping gain K_1 is varied at rated speed and no load. Note that No. 1-5 represent eigenvalues of fifth order state equation. In the conventional design method, the damping gain K_1 is decided to become multiple roots of No. 2 and No. 3 in order to suppress the overshoot of the motor speed. As shown in Fig. 3, the value of 0.15p.u. is the optimum value for the damping gain K_1. In addition, all roots are located in the left half of the s-plane; therefore, the system is stable.

From fifth-order state equation, the approximated second-order state equation is derived with the application of the following approximations, and expressed by (8):

1) under no-load condition; $\theta_0 = 0$, and $i_{\delta 0} = i_{\gamma 0} = 0$,
2) under high-speed condition; $\omega_0 L >> R$, and $\omega_0 >> K_1 i_{\delta 0}$,
3) mechanical time constant is sufficiently larger than electrical time constant; $p\Delta i_\gamma = p\Delta i_\delta = 0$,
4) root of HPF has small influence on the stability; $\Delta x = 0$.

$$p\begin{bmatrix}\Delta\omega\\ \Delta\delta\end{bmatrix}=\begin{bmatrix}0 & \dfrac{3}{2}\dfrac{P_f^{\,2}\psi_m^{\,2}}{JL_q}\\ -1 & -K_1\dfrac{\psi_m}{L_q}\end{bmatrix}\begin{bmatrix}\Delta\omega\\ \Delta\delta\end{bmatrix}+\begin{bmatrix}0\\ 1\end{bmatrix}\Delta\omega^* . \qquad (8)$$

It is noted that second-order state equation is derived under the condition of high-speed region and no load in order to simplify the analysis of the stability because the influence of load is relatively smaller than the influence of motor speed[(11)-(12)].

From (8), characteristic equation is expressed

$$s^2 + K_1\frac{\psi_m}{L_q}s + \frac{3}{2}\frac{P_f^{\,2}\psi_m^{\,2}}{JL_q} = 0, \qquad (9)$$

where s is the complex variable in Laplace transform.

Then, the damping coefficient ζ and the natural angular frequency ω_n are expressed by (10) and (11).

$$\zeta = \frac{\psi_m K_1}{2\omega_n L_q}. \qquad (10)$$

$$\omega_n = \sqrt{\frac{3}{2}}\frac{P_f\psi_m}{\sqrt{JL_q}}. \qquad (11)$$

As mentioned before, the damping gain K_1 is set in order to become multiple roots of No. 2 and No. 3.

On the other hand, the cutoff frequency ω_c of the HPF needs to be lower than the natural angular frequency ω_n in order to suppress the oscillation of the motor speed.

Fig. 4 shows the eigenvalue plot of the Motor A when the damping gain K_1 is varied under different cutoff frequency ω_c at rated speed and no load. In the figure, the root of No. 5 is on the real axis regardless of the damping gain K_1 when the cutoff frequency is set as 1/20 of the natural angular frequency ω_n.

From above considerations, the damping gain K_1 and the cutoff frequency ω_c are expressed by (12) and (13).

$$K_1 = \frac{2\omega_n L_q}{\psi_m}. \qquad (12)$$

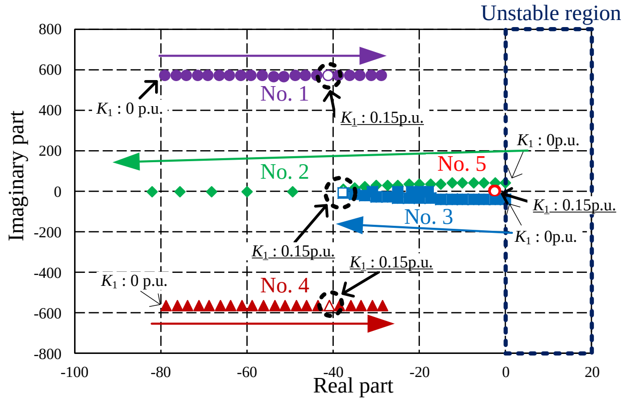

Fig. 3. Loot locus of fifth-order state equation when damping gain K_1 is increased at no-load and rated speed with Motor A.

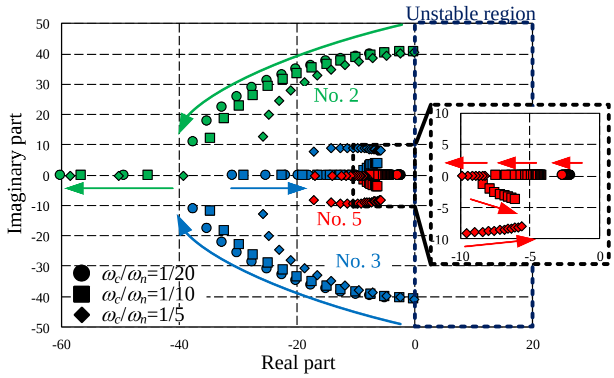

Fig. 4. Loot locus of fifth-order state equation under different cutoff frequency ω_c at no-load and rated speed.

$$\omega_c = \frac{\omega_n}{20} = \frac{1}{20}\sqrt{\frac{3}{2}}\frac{P_f\psi_m}{\sqrt{JL_q}}. \qquad (13)$$

It is noted that the damping coefficient ζ is set as 1 in (12).

2.3 Auto-tuning Method for Parameters of Conventional Damping Control In this section, an auto-tuning method for the conventional damping control is explained. In the auto-tuning, the parameters are identified in order to calculate the damping gain K_1 and cutoff frequency ω_c based on the equations (12) and (13).

The voltage command v_δ is expressed by

$$v_\delta^{\,2} = \left(\omega\psi_m + RI_a\right)^2 + \left(\omega L_q I_a\right)^2 . \qquad (14)$$

It is noted that the equation (14) is derived when $i_d = 0$ control is achieved. In addition, $I_a = i_q$ under $i_d = 0$ control.

From (14), the field flux linkage ψ_m is identified at the steady state by using

$$\hat{\psi}_m = \frac{\sqrt{v_\delta^{\,2} - \left(\omega^*\hat{L}_q I_a\right)^2} - \hat{R}I_a}{\omega^*}. \qquad (15)$$

Here, v_δ is the voltage command, $\hat{L}_q$ is the identified value of q-axis inductance, $\hat{R}$ is the identified value of winding resistance, I_a is the output current.

Next, the winding resistance R is identified in DC test at a standstill as (16).

$$\hat{R} = \frac{V_{DC}\left(D - f_{sw}T_d\right)}{1.5I_u} \quad \text{.......... (16)}$$

where D is the duty factor of the u-phase upper arm, and T_d is the dead-time.

The reactive power on the dq-axis is expressed by (17) under $i_d = 0$ control.

$$Q_{dq} = \omega L_q I_a^{\ 2} \quad \text{.......... (17)}$$

On the other hand, the reactive power on the γδ-axis is expressed by (18)

$$Q_{\gamma\delta} = v_\delta i_\gamma \quad \text{.......... (18)}$$

The reactive power on each axis is corresponded. Therefore, the identified q-axis inductance is expressed as (19) from (17) and (18).

$$\hat{L}_q = \frac{v_\delta i_\gamma}{\omega^* I_a^{\ 2}} \quad \text{.......... (19)}$$

The natural angular frequency is identified based on the hill-climbing method by injecting the sinusoidal wave into the speed command. The output current becomes the maximum value at the natural angular frequency. Therefore, the frequency of the injected sinusoidal wave is varied in order to search the maximum value of the output current.

Fig. 5 shows the flowchart of the auto-tuning. First, the winding resistance R is identified in DC test at standstill. Then, the motor is accelerated up to 0.5p.u. because it is impossible to identify the field flux linkage ψ_m and the q-axis inductance L_q at standstill as shown in (15) and (19). Next, the q-axis inductance L_q and the field flux linkage ψ_m are identified after applying maximum torque per ampere (MTPA) control based on the hill-climbing method[13]. The motor parameters are not necessary in the MTPA control because the operation point is searched by the relation of the output current. In addition, the natural angular frequency is identified by the relation between the frequency of the injected sinusoidal wave and the magnitude of the output current based on the hill-climbing method.

Fig. 6 shows the block diagram of the V/f control during the auto-tuning. From the figure, the motor is accelerated without the HPF of the damping control.

With this auto-tuning for the conventional damping control, the Motor A, which is stable with the conventional damping control, is stabilized.

2.4 Unstable Condition with Conventional Damping Control

Fig. 7 shows the eigenvalue plot of the Motor B when the damping gain K_1 is varied at the same condition of rated speed and no load. As shown in Fig. 7, the roots of No. 2 and No. 3 are multiple roots when the damping gain K_1 is 0.05p.u. However, the roots of No.1 and No.4 move into the right half of the s-plane. Therefore, these roots make the system unstable.

It is concluded from the above considerations that the Motor B becomes unstable due to the roots of No. 1 and No. 4 when the damping gain K_1 is decided by the conventional design method. It is noted that these roots are ignored when the fifth order state equation is linearized to second-order state equation.

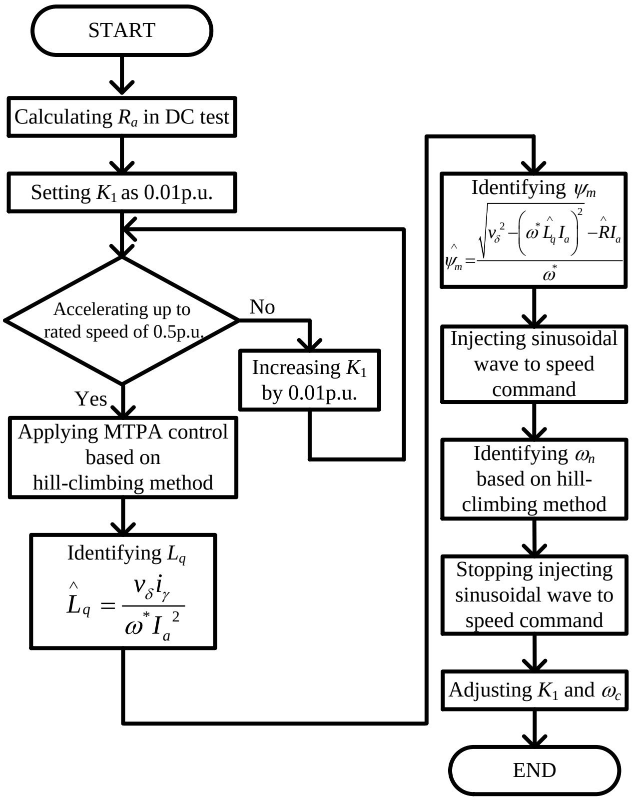

Fig. 5. Flowchart of auto-tuning method for conventional damping control based on V/f control.

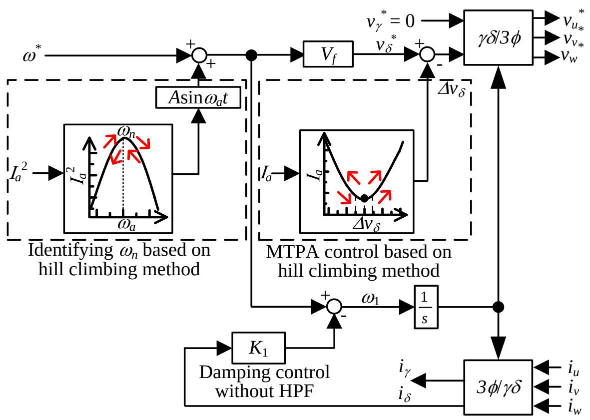

Fig. 6. Block diagram of V/f control when tuning parameters.

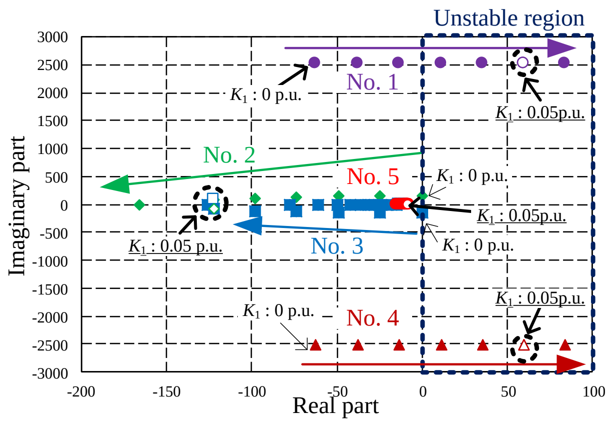

Fig. 7. Loot locus of fifth-order state equation when damping gain K_1 is increased at no-load and rated speed with Motor B.

2.5 Boundary Condition of Conventional Damping Control

In this section, the unstable condition with only the damping gain K_1 is derived. As mentioned before, the analysis is conducted at no load condition in order to simplify the analysis of the stability.

First, the fifth-order state equation is linearized into fourth-order state equation when the cutoff frequency is much smaller than the natural angular frequency of the second-order state equation. Then, the characteristic equation is expressed by (20).

$$s^4 + a_3 s^3 + a_2 s^2 + a_1 s + a_0 = 0, \quad (20)$$

where

$$a_3 = \frac{R}{L_d} + \frac{R}{L_q}, \quad (21)$$

$$a_2 = \omega_0{}^2 + \frac{3P_f{}^2 \psi_m{}^2}{2JL_q} + \frac{R^2}{L_d L_q}, \quad (22)$$

$$a_1 = K_1 \frac{\omega_0{}^2 \psi_m}{L_q} + \frac{3P_f{}^2 \psi_m{}^2 R}{2JL_d L_q}, \quad (23)$$

$$a_0 = \frac{3P_f{}^2 \omega_0{}^2 \psi_m{}^2}{2JL_q}. \quad (24)$$

Here, ω_0 is the steady state value of the motor speed.

From the equations (20)–(24) that the coefficients of the fourth-order characteristic equation are positive regardless of the value of the motor parameters. Therefore, the necessary condition of the Routh-Hurwitz stability criterion is satisfied. Thus, the unstable condition is derived from the Routh table.

Table 2 shows the Routh table which is acquired from the equations (20)–(24). The coefficients of the left end column are focused in order to evaluate the stability of the system. The unstable condition, where the coefficients b_1 and c_1 are negative, is expressed as (25) and (26).

$$\frac{L_d}{R} + \frac{L_d}{R}\frac{\omega_n{}^2}{\omega_0{}^2} + \frac{R}{L_q}\frac{1}{\omega_0{}^2} - \frac{\psi_m}{L_d + L_q}\left(\frac{L_d}{R}\right)^2 K_1 - \frac{3}{2}\frac{P_f{}^2 \psi_m{}^2}{J\left(L_d + L_q\right)}\frac{L_d}{R}\frac{1}{\omega_0{}^2} < 0. \quad (25)$$

$$b_1{}' \left\{ \frac{\psi_m}{R} K_1 + \frac{L_q}{L_d}\left(\frac{\omega_n}{\omega_0}\right)^2 \right\} - \frac{L_d + L_q}{R}\left(\frac{\omega_n}{\omega_0}\right)^2 < 0. \quad (26)$$

Here, $b_1{}'$ is the left-side term of the inequality equation (25).

It is concluded from the inequality equations (25), (26) and Tables 1–2, the left-side term are positive when the damping gain K_1 of 0.15p.u. is designed in the Motor A. On the other hand, $b_1{}'$, which is the left-side term of (26), is negative when the damping gain K_1 of 0.05p.u. is employed in the Motor B. Therefore, the system is unstable. These consequences are corresponded to the eigenvalue plots as shown in Figs. 3 and 6.

Fig. 8 shows the real parts of the roots of No. 1 and 4 when the damping gain K_1 is varied. The real parts $\alpha_{2,3}$ of No. 2 and No. 3 are expressed

$$\alpha_{2,3} = -\frac{K_1 \psi_m}{2L_q}. \quad (27)$$

Table 2. Routh table of fourth order state equation of V/f control with only damping gain K_1.

s^4	$a_4 = 1$	$a_2 = \omega_0{}^2 + \frac{3}{2}\frac{P_f{}^2 \psi_m{}^2}{JL_q} + \frac{R^2}{L_d L_q}$	$a_0 = \frac{3}{2}\frac{\omega_0{}^2 P_f{}^2 \psi_m{}^2}{JL_q}$
s^3	$a_3 = \frac{R}{L_d} + \frac{R}{L_q}$	$a_1 = K_1 \frac{\omega_0{}^2 \psi_m}{L_q} + \frac{3}{2}\frac{P_f{}^2 \psi_m{}^2}{JL_q}\frac{R}{L_d}$	0
s^2	$b_1 = \frac{a_3 a_2 - a_4 a_1}{a_3}$	a_0	0
s^1	$c_1 = \frac{b_1 a_1 - a_3 b_2}{b_1}$	0	0
s^0	a_0	0	0

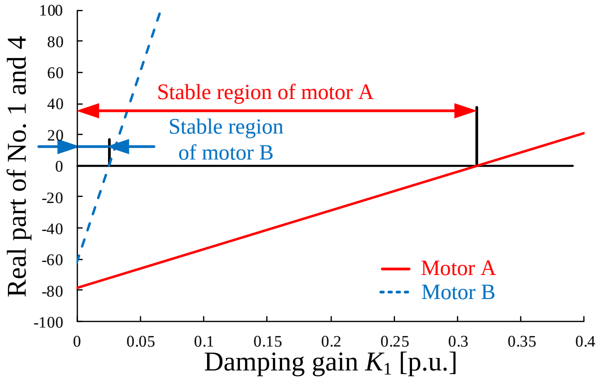

Fig. 8. Real part of No.1 and 4 when damping gain K_1 is increased under rated speed and no load.

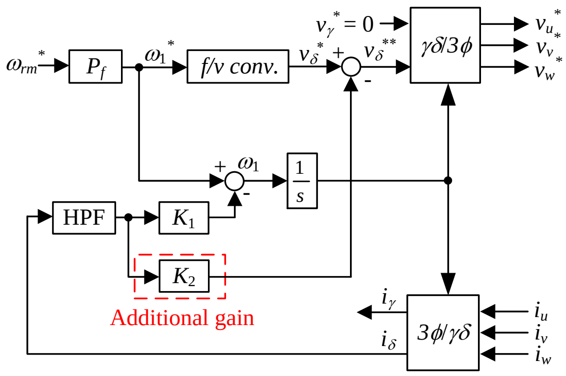

Fig. 9. Block diagram of V/f control based on γδ-frame with proposed feedback loop to output voltage command.

Then, the real parts $\alpha_{1,4}$ of No. 1 and No. 4 are expressed

$$\alpha_{1,4} = \frac{K_1 \psi_m}{2L_q} - \frac{R}{2}\left(\frac{1}{L_d} + \frac{1}{L_q}\right). \quad (28)$$

The real parts of No. 2 and No. 3 decrease proportionally to the damping gain K_1. On the other hand, the real parts of No. 1 and No. 4 increase proportionally to the damping gain K_1. Therefore, the stable condition is limited depending on the damping gain K_1. In addition, the stable region of the Motor B is smaller than that of the Motor A. In particular, the high-speed motor with small winding resistance is more apt to become unstable as expressed in (28). It is concluded from above considerations that there is unstable condition depending on the roots of No. 1 and No. 4. Therefore, a novel method is necessary in order to make the roots of No. 1 and No. 4 move into left-half of s-plane.

3. Proposed Additional Feedback Loop

3.1 Principle of Stabilizing Method with Additional Feedback Loop

Fig. 9 shows the control diagram of the V/f control with the novel feedback loop. As shown in Eq. (25), the third term in the left-side term of the inequality equation becomes larger when the winding resistance increases. Furthermore, the negative term, which is the fourth term, becomes smaller when the winding resistance increases. In other words, it is possible to stabilize the system when the term of the winding resistance is increased equivalently. Therefore, a novel feedback loop is added to the inverter voltage command v_δ^*. The feedback loop consists of an additional gain K_2 and the δ-axis current which is filtered by the HPF. Note that the definition of per unit value of K_2 is a quotient of rated voltage divided by rated current (Ω).

3.2 Stability Analysis with Additional Feedback Loop

The stability analysis is conducted under the same procedure in section 2.4. The unstable condition is derived from the Routh table. It is expressed as

$$\frac{L_d}{R}+\frac{L_d}{R}\frac{\omega_n^2}{\omega_0^2}+\frac{R+K_2}{L_q}\frac{1}{\omega_0^2}-\frac{\psi_m}{(R+K_2)L_d+RL_q}\frac{L_d^2}{R}K_1 -\frac{3}{2}\frac{P_f^2\psi_m^2}{J}\frac{R}{(R+K_2)L_d+RL_q}\frac{L_d}{R}\frac{1}{\omega_0^2}<0, \quad (29)$$

$$b_1^{''}\left\{\frac{\psi_m}{R}K_1+\frac{L_q}{L_d}\left(\frac{\omega_n}{\omega_0}\right)^2\right\}-\frac{(R+K_2)L_d+RL_q}{R^2}\left(\frac{\omega_n}{\omega_0}\right)^2<0. \quad (30)$$

where $b_1^{''}$ is the left-side term of (29).

It is shown in (29) that the additional gain K_2 is added to the numerator of the third term in left-side by adding new feedback loop. In addition, the denominators of the fourth and fifth terms are also increased by the additional gain K_2. Therefore, the winding resistance is equivalently increased by the additional gain K_2 in order to stabilize the system.

Fig. 10 shows the eigenvalue plot when K_2 is increased at the rated speed and no load. It is noted that the damping gain K_1 is decided as multiple roots of No. 2 and No. 3. The roots of No. 1 and No. 4 move into the left side of s-plane in accordance with the increase of the additional gain K_2. This stabilization is not achievable with only damping gain K_1.

4. Experimental Results

4.1 Auto-tuning for Conventional Damping Control

In this section, the effectiveness of the auto-tuning method for the conventional damping control is confirmed in the experiment with the Motor A. It is noted that the DC test is conducted at standstill. In addition, even though the dead-time has not been considered in the analysis, the dead-time influence appears as the larger winding resistance in the experiment. Therefore, in the experiment, the system might become stable even in the unstable region in the root locus analysis result. In order to ignore this stable region difference between the experimental result and analysis result, the other parameters are identified under the condition of a rated speed of 0.5p.u. and a rated torque of 0.27p.u.

Fig. 11 shows the waveform of the DC test. The identified value of the winding resistance converges to the nominal value in the steady state. In general, winding resistance of a general-purpose motor is relatively small. Therefore, the duty ratio is set as 5% in order to prevent overcurrent in the test. From the figure, the winding resistance is identified with an error of 9.6%.

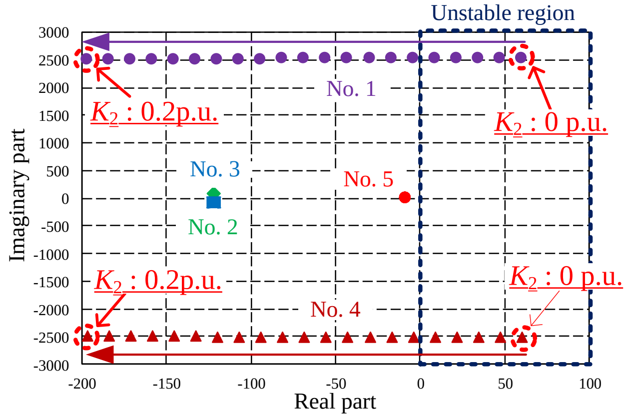

Fig. 10. Root locus when damping gain K_2 is increased under rated speed and no load with Motor B.

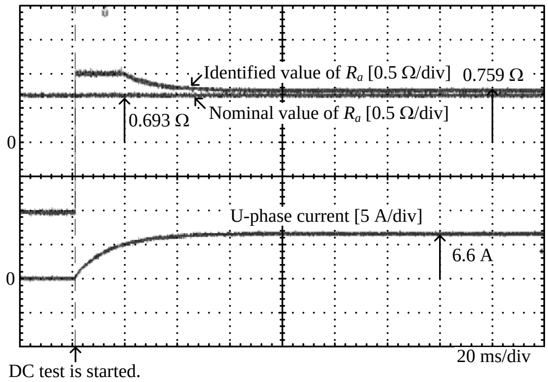

Fig. 11 Waveforms of DC test.

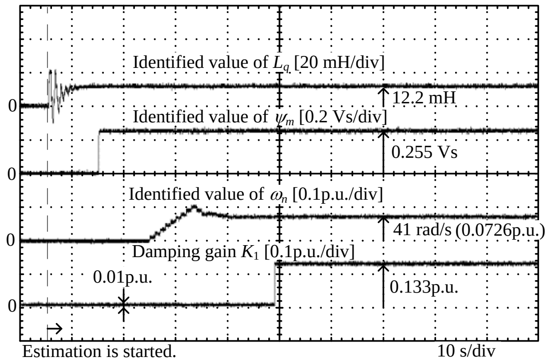

Fig. 12 Waveforms of auto-tuning each parameter.

Fig. 12 shows each identified parameter and calculated damping gain K_1. From the figure, the identification and the calculation are conducted in 44 s. The frequency of the injected sinusoidal wave is varied each 1 Hz in the identification of the natural angular frequency. In addition, one period of the sinusoidal wave needs to be injected at least. Thus, the injecting time of the sinusoidal wave on each frequency is set as 1 s. Therefore, the tuning time of the natural angular frequency is relatively long compared with the other parameters.

Fig. 13 shows the step response before and after the auto-tuning. In Fig. 13 (a), the damping gain is set as 0.01p.u. In addition, the HPF of the damping control is not utilized. On the other hand, the damping gain K_1 is set as 0.13p.u. and the cutoff frequency is 1/20 of the identified natural angular frequency. In the figure, the motor speed oscillates when the step speed command is employed before applying the auto-tuning. In addition, the steady-state error remains in the motor speed because the HPF is not implemented. On the other hand, the motor speed follows the command without an overshoot.

Fig. 14 shows the step responses with the optimal damping gain and the tuned damping gain. From the figure, the overshoot with the tuned damping gain is almost same as the optimal damping gain.

Through the experimental results, the effectiveness of the auto-tuning method is confirmed.

4.2 Stabilization with Additional Feedback Loop In order to confirm the validity of the additional feedback loop, the experiment is conducted. It is noted that Motor A which is shown in Table 1 is used in the experiment. In addition, inductors of 10 mH are connected in series in order to evaluate the motor with the long time constant.

Fig. 15 shows the waveforms of γ, δ-axis current and U-phase current at 0.9p.u. of rated speed and 0.7p.u. of rated torque when the damping gain K_1 is varied from 0.1p.u. to 0.2p.u. Note that the additional gain K_2 is set as 0 at this condition. The diverging oscillation occurs in γ, δ-axis current after the damping gain K_1 is varied to 0.2p.u. Then, the motor is stopped due to the overcurrent detection. Each frequency of the oscillation is 81 Hz and 78 Hz, whereas, the frequency which is obtained from the eigenvalue plot is 81 Hz. The experimental value agrees with the theoretical value with error of 5.5%. As a conclusion, the system with the motor, of which electrical time constant is long, easily becomes unstable only with the conventional damping gain K_1 due to the influence of the ignored roots depending on K_1.

Fig. 16 shows the waveforms of γ, δ-axis current and U-phase current at 0.9p.u. of rated speed and 0.7p.u. of rated torque when the additional gain K_2 is varied. The system is stabilized by the additional gain K_2 even under the unstable condition with only the damping gain K_1. In addition, the current ripple is also suppressed by the additional gain K_2.

From the experimental results, the effectiveness of the additional feedback loop is confirmed.

5. Conclusion

In this paper, the designing method for the conventional damping control is explained. In addition, the auto-tuning method is introduced for the motor which is stable with the conventional damping control. Then, the unstable condition due to the damping gain K_1 is derived based on the state equation regarding the V/f control for IPMSMs. From the unstable condition, it is clarified that the high-speed motor, which the electrical time constant is long, is apt to be unstable. The validity of the analysis is confirmed by the eigenvalue plot and the experiment. In order to solve this instability problem, the novel feedback loop is added to the inverter voltage command in order to increase the winding resistance. As a result, the stable condition is achieved by the additional equivalent resistance gain K_2 even under the unstable condition with only damping gain K_1. In the experiment, first, the effectiveness of the

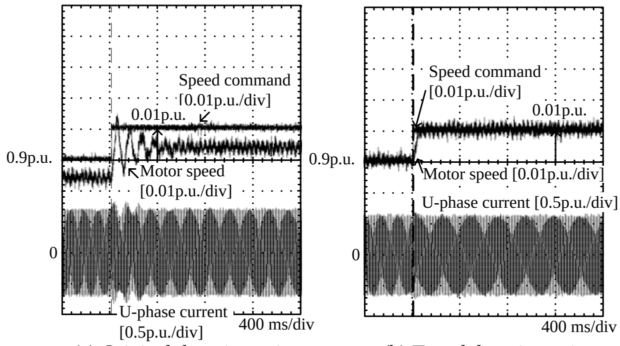

(a) Original damping gain without HPF. (b) Tuned damping gain with HPF.

Fig. 13 Waveforms of step response before and after auto-tuning under 0.9p.u. of rated speed and 0.8p.u. of rated torque.

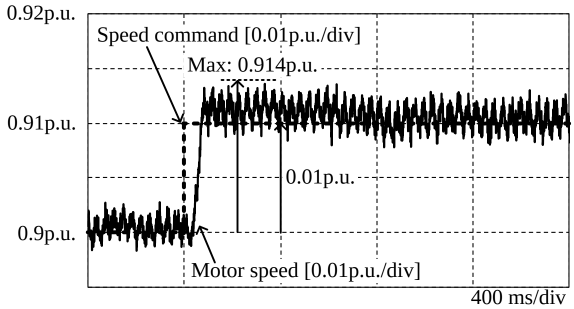

(a) With optimal damping gain (K_1 = 0.16p.u.).

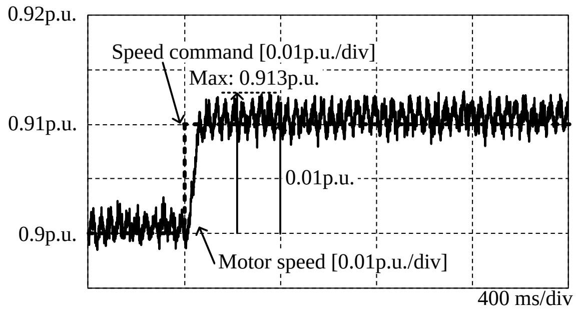

(b) With tuned damping gain (K_1 = 0.13p.u.).

Fig. 14 Waveforms of step response with different damping gain K_1 under 0.9p.u. of rated speed and 0.8p.u. of rated torque.

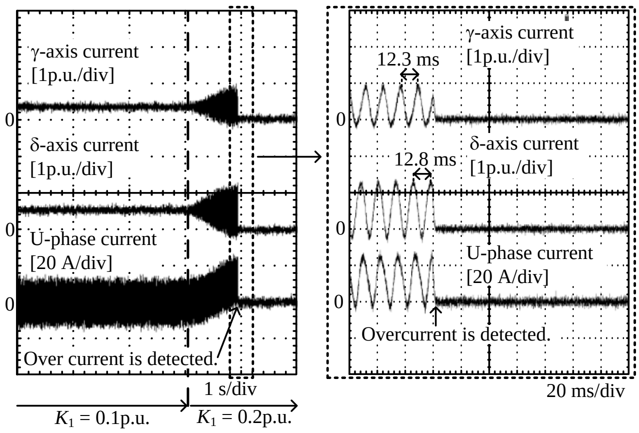

Fig. 15. Operation waveform without feedback loop K_2 when damping gain K_1 is varied from 0.1p.u. to 0.2p.u. under 0.9p.u. of rated speed and 0.7p.u. of rated torque.

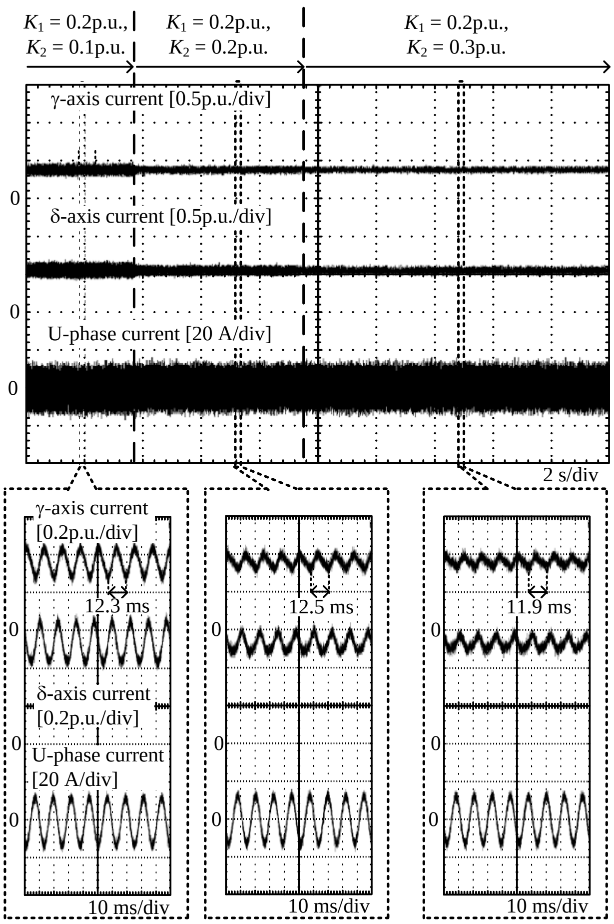

Fig. 16. Waveforms when additional gain K_2 is varied under 0.9p.u. of rated speed and 0.7p.u. of rated torque.

auto-tuning for the conventional damping control is confirmed. Next, the effectiveness of K_2 is confirmed under 0.9p.u. of rated speed and 0.7p.u. of rated torque.

References

(1) K. Kondo, S. Doki : "Position Estimation System for PMSM Position Sensorless Control in Inverter Overmodulation Drive," *IEEJ J. Ind. Appl.*, Vol.6, No.3, pp.165-172, 2017.

(2) R. Takahashi, K. Ohishi, Y. Yokokura, H. Haga, T. Hiwatari : "Stationary Reference Frame Position Sensorless Control Based on Stator Flux Linkage and Sinusoidal Current Tracking Controller for IPMSM," *IEEJ J. Ind. Appl.*, Vol.6, No.3, pp.181-191, 2017.

(3) A. Shinohara, Y. Inoue, S. Morimoto, M. Sanada : "Correction Method of Reference Flux for Maximum Torque per Ampere Control in Direct-Torque-Controlled IPMSM Drives," *IEEJ J. Ind. Appl.*, Vol.6, No.1, pp.12-18, 2017.

(4) R. Tanabe, K. Akatsu : "Advanced Torque and Current Control Techniques for PMSMs with a Real-time Simulator Installed Behavior Motor Model," *IEEJ J. Ind. Appl.*, Vol.5, No.2, pp.167-173, 2016.

(5) X. Ji, T. Noguchi : "Online q-axis Inductance Identification of IPM Synchronous Motor Based on Relationship between Its Parameter Mismatch and Current," *IEEJ J. Ind. Appl.*, Vol.4, No.6, pp.730-731, 2015.

(6) M. Miyamasu, K. Akatsu : "Efficiency Comparison between Brushless DC Motor and Brushless AC Motor Considering Driving Method and Machine Design," *IEEJ J. Ind. Appl.*, Vol. 2, No.1, pp.79-86, 2013.

(7) P. D. Chandana Perera, F. Blaabjerg, John K. Pederson, P. Thøgersen : "A sensorless, Stable V/f Control Method for Permanent-Magnet Synchronous Motor Drives," *IEEE Trans. on Ind. Appl.*, Vol. 39, No. 3, pp. 783-791, 2003.

(8) G. L. Kruger, A. J. Grobler, S. R. Holm : "Improved non-ideality compensation for the V/f controlled permanent magnet synchronous motor," in *Conf. Proc. Industrial Technology*, pp. 331-336, 2013.

(9) J. Itoh, N. Nomura, H. Ohsawa: "A comparison between V/f control and position-sensorless vector control for the permanent magnet synchronous motor," in *Conf. Proc. Power Conversion Conf.*, Vol. 3, pp. 1310-1315, 2002.

(10) D. Sato, J. Itoh: "Open-loop control for permanent magnet synchronous motor driven by square-wave voltage and stabilization control," in *Conf. Proc. Energy Conversion Congress and Exposition*, EC-0319, 2016.

(11) Motion Control, INTECH, pp. 439-458, 2010.

(12) Z. Tang, X. Li, S. Dusmez, B. Akin : "A New V/f Sensorless MTPA Control for IPMSM Drives," *IEEE Trans. on Power Electron.*, Vol. 31, No. 6, pp. 4400-4415, 2016.

(13) J. Itoh, T. Toi, M. Kato : "Maximum Torque per Ampere Control Using Hill Climbing Method Without Motor Parameters Based on V/f Control," in *Conf. Proc. European Conference on Power Electronics and Applications*, DS3d-Topic40283, 2016.

Jun-ichi Itoh

(Senior member) received his M.S. and Ph.D. degree in electrical and electronic systems engineering from Nagaoka University of Technology, Niigata, Japan in 1996, 2000, respectively. From 1996 to 2004, he was with Fuji Electric Corporate Research and Development Ltd., Tokyo, Japan. He was with Nagaoka University of Technology, Niigata, Japan as an associate professor. Since 2017, he has been a professor. His research interests are matrix converters, dc/dc converters, power factor correction techniques, energy storage system and adjustable speed drive systems. He received IEEJ Academic Promotion Award (IEEJ Technical Development Award) in 2007. In addition, he also received Isao Takahashi Power Electronics Award in IPEC-Sapporo 2010 from IEEJ, 58th OHM Technology Award from The Foundation for Electrical Science and Engineering, November, 2011, Intelligent Cosmos Award from Intelligent Cosmos Foundation for the Promotion of Science, May, 2012, and Third prize award from Energy Conversion Congress and Exposition-Asia, June, 2013. Prizes for Science and Technology (Development Category) from the Commendation for Science and Technology by the Minister of Education, Culture, Sports, Science and Technology, April 2017. He is a senior member of the Institute of Electrical Engineers of Japan, the Society of Automotive Engineers of Japan and the IEEE.

Takato Toi

(Member) received his B.S. and M.S. degrees in electrical, electronics and information engineering from Nagaoka University of Technology, Niigata, Japan in 2016 and 2018, respectively. Since 2018, he has been with Mitsubishi Electric Corporation, Japan. He is a member of IEEJ and IEEE. His research interests include PM motor drives.

Koroku Nishizawa

(Student member) received his B.S. degree in electrical, electronics and information engineering from Nagaoka University of Technology, Niigata, Japan in 2015. And he has been in 5-year integrated doctoral course of Nagaoka University of Technology. He is the student member of IEEJ and IEEE. His research interests include PM motor drives and modulation method of power converters.